Low Frequency Near Field Interferometry for Characterization of Lossy Dielectric and an Investigation on Sea Ice

M. Shifatul Islam, Sadman Shafi, Md. Imrul Hasan and Mohammad Ariful Haque

***Abstract*—The far field interferometry is a well established method of subsurface characterization, and it has traditionally been used to determine the dielectric properties and thickness of very low-loss subsurface materials, whose dimensions are comparable to the operating wavelength. However, this method is not very well suited for dielectrics with losses several orders high and therefore cannot be considered as a general method of subsurface characterization. In this paper, we introduce a new idea of near field interferometry, which can be used to characterize higher-loss dielectrics with dimensions very low compared to the wavelength. It is shown that in low frequencies, there is a noticeable variation in the field components with different medium dielectric properties and thickness, and these changes can be detected externally from near-field measurements by varying receiver distance and the operating frequency. The proposed method is tested on a lossy sea ice model in the presence of a horizontal electric dipole, and variation in field magnitudes is observed for thickness up to 5 meters. Since practical sea ice bulks have thicknesses of similar range, the near-field interferometry appears to be a promising approach to determine sea ice thickness from non-invasive measurements.**

***Index Terms*—characterization, interferometry, Sommerfeld integral, layered media, lossy dielectric, dipole radiation, near-field, low-frequency.**

I. Introduction

THE method of interferometry involves measuring the electrical properties of a dielectric material, e.g., geophysical subsurface and changes in the subsurface thickness with the help of wave interference (mostly by spherical wave sources). The subsurface is usually a very low conductive dielectric material, terminated by a semi-infinite halfspace. In practice, a source is kept over the terrestrial surface, and a radial sweep of the receiver antenna is performed over a particular distance of interest. This sweep results in an interference pattern, including several maxima and minima, and a noticeable variation is observed in the magnitude profile. Investigating the pattern and the magnitudes, one can obtain good enough estimate of the subsurface thickness, as well as both the dielectric constant and the loss behaviours [1], [2]. Over the past, this method has been used to investigate regions with low loss such as layered earth [3], terrestrial ice glaciers [4], lunar sample model [5], or very thick or dense vegetation layer [6]. The analytical model of these environments is assumed to be a three layered system [1], where the upper medium is the source air medium, the middle layer is the subsurface of particular interest and the bottom layer is a semi infinite ground, usually of very high conductive loss. The measured electric and magnetic field intensities in the far-field region show distinctive magnitude profiles [2], [4], [5], [7] and in general agree significantly with those obtained through analytical and computational results.

The changes in field patterns and values with subsurface properties has been extensively studied in [2], both analytically and experimentally. It is shown that with the increase of dielectric constant, the magnitude vs radial distance profile tends to shift downwards but the patterns keep their integrity and smooth out only slightly. However, with increasing loss tangent of the subsurface, the patterns not only shift downwards but also they tend to smooth out. It is also observed that as the thickness gets thinner compared to the wavelength, the maxima and minima tend to become less distinctive. Both of these observations make the far field interferometry a very unattractive technique for characterizing higher lossy dielectrics with thickness much less than the wavelength. The simulations of [8] also suggest that the patterns are also not very well-distinctive if a multilayered system is not terminated by good conductors.

The analytical treatment of the fields in the presence of a layered medium needs a highlight as well. The problem was first addressed by Sommerfeld [9], who used the Hertz potential and decomposed the spherical potential field into an integral superposition of a cylindrical and a planewave components, famously known as the Sommerfeld identity [9]–[11]. Since reflective nature of the layered medium under consideration is represented in the planewave reflection coefficients, such approach enables us to use these coefficients to determine the fields in the presence of the layered medium. The traditional problem became mathematically sophisticated through the works of [1]–[3], [12], [13]. [13] presented the mathematical formulation of reflection coefficients of a multilayered medium through surface impedances and used his work to evaluate the far field components over lossy half space grounds. The traditional Hertzian potential approach was abandoned in the more modern works, and Tsang, Kong, Chew et al. [5], [10], [14], [15] used the Sommerfeld identity together with the spherical Green's function of a point source to directly convert the electric and magnetic fields of a point

M. Shifatul Islam is with Anyeshan Limited, Dhaka, Bangladesh. E-mail: shifatul@anyeshan.com

Sadman Shafi and Md. Imrul Hasan are with Anyeshan Limited, Dhaka, Bangladesh.

Mohammad Ariful Haque is with the Department of Electrical and Electronic Engineering, Bangladesh University of Engineering and Technology, Dhaka, Bangladesh.

dipole into cylindrical coordinates. The expressions of reflection coefficients are obtained from the boundary conditions at each layer interface. The approach greatly simplified the cumbersome Hertzian potential approaches, and allowed the direct use of integral equations for any dipole orientation. Later [16], [17] gave a complete shape to the problem in their works considering arbitrary positions of source and receivers, with the additional inclusion of medium anisotropy as well. The inclusion of the Sommerfeld identity enabled the analysis of antenna in the presence of medium inhomogeneity, and direct expressions of the field components became obtainable. However, the identity itself is an integral of complex numbers, and proper methods for evaluation of these integral expressions also became a parallel branch of interest.

In these works, the fields considered were in the far field region. In the far field, Hankel functions in the integral expressions have a closed form representation [1], [10], [18]. In addition, the contributions of those cylindrical and planewave components are dominated by only one particular component, which is the direct ray contribution from the source to the receiving point. These two advantages in the far field allowed the whole source-receiver interaction to be modeled as contribution of two discrete rays; the dominant incident and reflected rays, giving rise to the famous Geometrical Optics Approximation (GOA) [1], [4], [7], [8], [12]–[14], [19], [20]. That particular dominant wave component can be found using the saddle point method [1], [8], [12], [19], and therefore GOA enabled the computation of field values in the far field. Later on, GOA was refined in [4], [7] with the inclusion of uniform asymptotic methods [21]–[23]. However, these approximations show very poor results for the near field cases. With the availability of stronger computers later on, numerical approaches started to gain more highlight due to their flexibility and accuracy in both near and far fields and gradually replaced these asymptotic methods [4], [10], [20].

The numerical integration using standard quadratures (such as Simpson's rule) is quite challenging. This is due to the oscillatory nature of the Bessel functions in the integral and possible locations of poles and branch points near the integration path. Chew [10] provided a robust integration path parallel to the real k axis, which is in the fourth quadrant of the integrand plane (k will have a negative imaginary part). However, the choice of this negative value is not arbitrary, as shown by [24]. The additional requirement to sample the oscillatory functions at higher frequencies and large receiver distances make the traditional numerical approaches very cumbersome although the results obtained are correct. [8], [25], [26] involved the use of the Discrete Fourier Transform (DFT) for computing the integral, which is considerably faster than the standard quadrature methods. However, it needs a very large number of DFT points for large distances and frequencies. On the other hand, the quadrature methods converge very fast at low frequencies and/or high receiver heights. Both of these methods promise very efficient means of numerical techniques to evaluate the field integrals. The speed of the quadrature methods can be improved by adaptive methods, such as Filon quadrature [27], [28] and Romberg's method [29] within the zeros of the Bessel functions [30]. In recent years, Hunziker et al. [31]–[34] proposed the use of Gauss-Kronrod quadrature as an efficient numerical tool to evaluate the field patterns in both near and far regions. The method, despite being very fast, requires a proper tuning of some internal parameters to assure convergence and accuracy.

In our work, we have shifted the attention from the far field to the near field case, for antennas operating in the MHz range. In the near field realm, maxima and minima patterns do not exist for low thickness subsurfaces. However, we show that the field magnitude itself has a significant variation with the variation of subsurface thickness and dielectric properties. As a result, the near field interferometry can be a promising method of subsurface characterization. The rest of the paper is divided into 4 sections. In section II we discuss the mathematical expressions of the electric and magnetic field components of a horizontal electric dipole. In section III, we describe the Simpson's and DFT methods for computing the field components. In section IV, we first discuss the near field patterns with variation of medium dielectric properties, loss and thickness, along with some detailed interpretation and limitations; then discuss the feasibility of the method on a layered sea ice model presented in [35]. Finally, in section V, general remarks will be drawn and the possibility of further work will be discussed.

II. Mathematical expressions of fields in layered media

In our work, we have assumed a horizontal electric dipole to be the source of radiation. We use the convention that $\hat{z}$ is directed upwards. The dipole is located at the origin, with its dipole moment in the $\hat{x}$ direction, and placed above a system of an n layered medium. The arrangement is shown in Fig. 1. The dipole is located in air – which we call the source medium (0th layer). There are n horizontal interfaces located at $z = d_0; d_1; d_2 ::: d_{n-1}$, where, by convention of the z-axis, $d_0; d_1; d_2; ::: d_{n-1} \quad 0$. The 0th and the nth (bottom) layers are semi-infinite. The source is placed on the air-medium 1 interface ($d_0 = 0$). The time dependence of the fields is represented by $e^{i!t}$. We can decompose the spherical wave propagating in the mth layer into cylindrical and planewave components using the Sommerfeld identity as below

$$\frac{e^{ik_m r}}{r} = \int_0^{\infty} \frac{k}{k_{z;m}} H_0^1(k\ ) e^{ik_{z;m} z} dk \qquad (1)$$

where $r = \sqrt{\ ^2 + z^2}$ is the distance from the dipole to the receiver at the point with cylindrical coordinates $(\ ; \ ; z)$. $H_0^1(x)$ is the Hankel function of the first kind with order 0. $\tilde{k_m}$ is the spherical wave propagation vector in medium m that can be expressed in terms of its components in the cylindrical system; with one component as a tangential cylindrical wave with propagation vector $\vec{k} = k\ \hat{}$ and the other component as a vertical plane wave with propagation vector $\vec{k}_{z;m} = k_{z;m}\hat{z}$ and therefore we can write

$$\vec{k}_m = k\ \hat{} + k_{z;m}\hat{z}: \qquad (2)$$

In this convention, $k_m; \ k\ ; \ k_{z;m}$ should have a positive imaginary part to ensure radiation condition, and a positive real

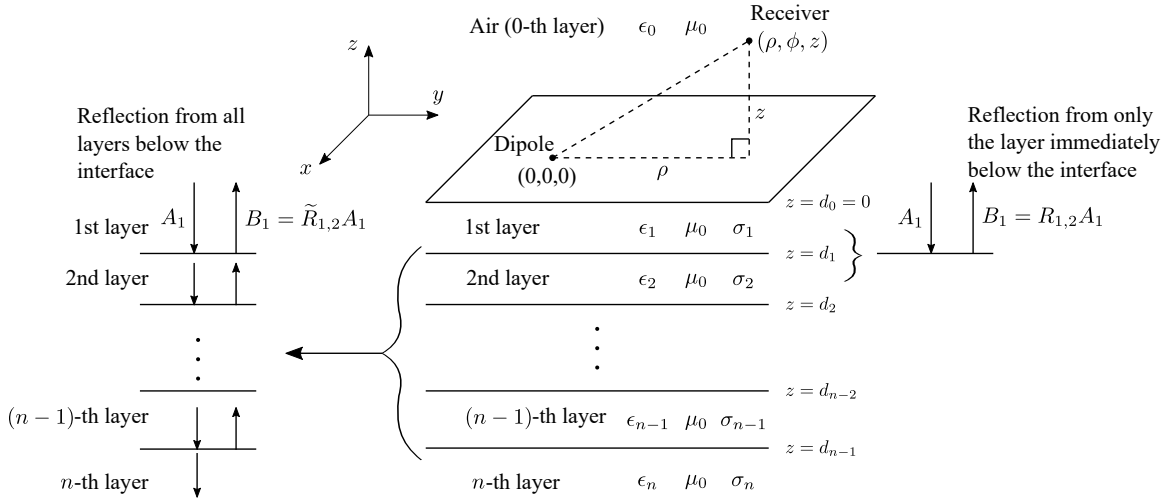

Fig. 1. Schematic of a horizontal dipole radiating over a layered medium (layer 1 to n 1), terminated by a half space (layer n)

part indicates propagation along the $+z$ axis. The governing equations for the transverse magnetic (TM) components, $\vec{E}^{TM}$ and $\vec{H}^{TM}$, of the electric and magnetic fields (see [5], [15]) at (; ;z) are

$$\vec{E}^{TM} = \int_1^{\infty} \frac{Il}{8\omega} \begin{bmatrix} ik_z k \left[1 + \tilde{R}^{TM} e^{ik_z z}\right] H_1^{(1)'}(k\rho)\cos\phi \\ \frac{k_z}{\rho}\left[1 + \tilde{R}^{TM} e^{ik_z z}\right] H_1^{(1)}(k\rho)\sin\phi \\ k^2\left[1 + \tilde{R}^{TM} e^{ik_z z}\right] H_1^{(1)}(k\rho)\cos\phi \end{bmatrix} dk \tag{3a}$$

$$\vec{H}^{TM} = \int_1^{\infty} \frac{Il}{8} \begin{bmatrix} \frac{1}{\rho}\left[1 + \tilde{R}^{TM} e^{ik_z z}\right] H_1^{(1)}(k\rho)\sin\phi \\ k\left[1 + \tilde{R}^{TM} e^{ik_z z}\right] H_1^{(1)'}(k\rho)\cos\phi \\ 0 \end{bmatrix} dk \tag{3b}$$

While the transverse electric (TE) components, $\vec{E}^{TE}$ and $\vec{H}^{TE}$, are

$$\vec{E}^{TE} = \int_1^{\infty} \frac{Il\omega}{8} \begin{bmatrix} \frac{1}{k_z}\left[1 + \tilde{R}^{TE} e^{ik_z z}\right] H_1^{(1)}(k\rho)\cos\phi \\ \frac{k}{k_z}\left[1 + \tilde{R}^{TE} e^{ik_z z}\right] H_1^{(1)'}(k\rho)\sin\phi \\ 0 \end{bmatrix} dk \tag{3c}$$

$$\vec{H}^{TE} = \int_1^{\infty} \frac{Il}{8} \begin{bmatrix} ik\left[1 + \tilde{R}^{TE} e^{ik_z z}\right] H_1^{(1)'}(k\rho)\sin\phi \\ \frac{i}{\rho}\left[1 + \tilde{R}^{TE} e^{ik_z z}\right] H_1^{(1)}(k\rho)\cos\phi \\ \frac{k^2}{k_z}\left[1 + \tilde{R}^{TE} e^{ik_z z}\right] H_1^{(1)}(k\rho)\sin\phi \end{bmatrix} dk \tag{3d}$$

Here,

l = length of the hertzian dipole , the operating wavelength

I = Driving current of the dipole

ω = 2 f = Angular frequency of the driving current

= permittivity of the source medium (= $_0$)

= Azimuth angle of the receiver point, measured from the positive x axis. For a horizontal dipole oriented along the positive x axis, = 0 corresponds to the endfire direction and = 90 corresponds to the broadside direction.

z = Height of the receiver. The receiver is at the source medium, therefore z 0.

$\tilde{R}^{TM}$, $\tilde{R}^{TE}$ = Generalized reflection coefficients of the stratified medium for TM and TE plane waves looking from the source medium.

$H_1^{(1)}(k\rho)$ = Hankel function of first kind in $k\rho$ with order 1. $H_1^{(1)'}(k\rho)$ is its first derivative.

Also, for the source medium (layer 0),

$$k_z = \sqrt{k^2 - k^2}$$

In our discussions, we will use the subscript m to denote the electrical properties and the propagation vectors in medium m. However, for compactness, we will ignore the subscripts in the source medium (excepting the permittivity and permeability, for which we will use the conventional symbols $_0$ and $_0$). Therefore, $\vec{k}$ is the wave propagation vector in the source medium, k_z is the z component of it. The Hankel functions of the first kind are related with the Bessel and Neumann functions with the following relation:

$$H^{(1)}(x) = J (x) + iN (x)$$

$J (x)$ and $N (x)$ are the Bessel and Neumann functions of order . Such integral representation for all other dipole configurations is available in [15]. For brevity, we can observe that each of the integrands in (3) is of the form

$$F = \int_1^{\infty} h(k\rho)\,\mathrm{H}(k\rho)\,dk \tag{4}$$

$h(k\rho)$ can be even or odd functions of $k\rho$. And for horizontal electric dipole, $\mathrm{H}(k\rho)$ can have the these two forms - $H_1^{(1)}(k\rho)$ or $H_1^{(1)'}(k\rho)$. We can use the following formulas

to remove the derivatives of the Hankel functions from the integrals.

$$H_0^{(1)'}(k\ ) = -H_1^{(1)}(k\ ) \tag{5a}$$

$$H_1^{(1)'}(k\ ) = H_0^{(1)}(k\ ) - \frac{1}{k}H_1^{(1)}(k\ ) \tag{5b}$$

Once the integrals are expressed in terms of Hankel functions, each of the integral terms of (3) are expressed in the following form

$$F_1 = \int_1^{\infty} h_1(k\ ) H^{(1)}\ (k\ )\, dk\ ; \quad = 0;1 \tag{6}$$

which can be folded [14], [20] to

$$F_2 = 2\int_0^{\infty} h_1(k\ ) J\ \ (k\ )\, dk\ ; \quad = 0;1 \tag{7}$$

The later representation has the advantage that it bypasses the singularity of the Hankel function at the origin, and at the same time reduces computation time for the numerical integration.

The information of the subsurface is embedded in the reflection coefficients, namely in $\tilde{R}^{TM}$ and $\tilde{R}^{TE}$. The generalized TM reflection coefficient at the mth interface considering the effects of the mth layer and all the layers below it is (see [10])

$$\tilde{R}^{TM}_{m;\ m+1} = \frac{R^{TM}_{m;\ m+1} + \tilde{R}^{TM}_{m+1;m+2} e^{\ -2ik_{z;m+1}h_{m+1}}}{1 + R^{TM}_{m;\ m+1}\tilde{R}^{TM}_{m+1;m+2} e^{\ -2ik_{z;m+1}h_{m+1}}} \tag{8}$$

where $R^{TM}_{m;m+1}$ is the Fresnel reflection coefficient at the mth interface considering the effects of the mth and $(m+1)$th layers only (see Fig. 1). Specifically,

$$R^{TM}_{m;m+1} = \frac{{}_{m+1}\ \ i\frac{{}_{m+1}}{!}\ k_{z;m} \quad - \ {}_{m}\ \ i\frac{{}_{m}}{!}\ k_{z;m+1}}{{}_{m+1}\ \ i\frac{{}_{m+1}}{!}\ k_{z;m} + \ {}_{m}\ \ i\frac{{}_{m}}{!}\ k_{z;m+1}} \tag{8a}$$

Here,

${}_m = {}_{m;r}\ {}_0$ = real permittivity of layer m. ${}_{m;r}$ is the dielectric constant

${}_m$ = Equivalent electrical conductivity of layer m [15]

Since there are no other media after the nth layer, only the effects of the $(n-1)$th and the nth layers will be present in the reflection coefficients ($R^{TM}_{n-1;n} = \tilde{R}^{TM}_{n-1;\ n}$). Using this fact, we can compute $\tilde{R}^{TM}_{n-2;\ n-1}$; $\tilde{R}^{TM}_{n-3;\ n-2}, \ldots; \tilde{R}^{TM}_{2;3}$; $\tilde{R}^{TM}_{1;2}$; $\tilde{R}^{TM}_{0;1}$ recursively using (8) and find out $\tilde{R}^{TM} = \tilde{R}^{TM}_{0;1}$.

The computation of R^{TE} involves a similar procedure that uses (8), with $R^{TE}_{m;m+1}$ and $\tilde{R}^{TE}_{m;m+1}$ replacing $R^{TM}_{m;m+1}$ and $\tilde{R}^{TM}_{m;m+1}$ respectively. Also, instead of using (8a), we use the following equation for $R^{TE}_{m;m+1}$

$$R^{TE}_{m;m+1} = \frac{{}_{m+1}k_{z;m} \quad - \ {}_{m}k_{z;m+1}}{{}_{m+1}k_{z;m} + \ {}_{m}k_{z;m+1}}$$

Usually the materials of interest are nonmagnetic, therefore ${}_m = {}_{m+1} = {}_0$. So,

$$R^{TE}_{m;m+1} = \frac{k_{z;m} - k_{z;m+1}}{k_{z;m} + k_{z;m+1}} \tag{8b}$$

III. Numerical methods for computing field components

Numerical evaluation of the integrals of the forms in (4) and (7) is not a straightforward process. The oscillatory nature of the Bessel functions increases with increasing frequency and radial distance, and therefore the sampling density of the integrand has to be increased. The possible proximity of the poles and branch points of the function $h(k\ )$ near the path of integration also make the straightforward treatment of the integrands intractable.

Fig. 2 shows the location of the poles, branch points and branch cuts of the integrands in (4) and (7) in the complex $k = k_r + ik_i$ plane, where $k_r = \mathrm{Re}\{k\}$ and $k_i = \mathrm{Im}\{k\}$. The poles are mainly of two types. The first type involves the values of k, which set the denominator of the right hand side of (8) to zero, commonly known as the guided mode poles, and the second type involves the case when the denominator of (8a) is set to zero, commonly known as TM poles or Sommerfeld poles [1], [5], [7], [12]. In addition, the Hankel functions have a singular point at the origin. All the poles are located in the first quadrant of the complex k plane [10].

The branch cuts, or branch lines are lines in the complex plane cutting through which (while traversing a path in the plane) will alter the sign of k_z, and the branch points are the points from which those cuts emanate. For a source at free space, the branch point under consideration is at $k = k$, and two branch cuts emerge out of it. These two branch cuts constitute the hyperbola $\mathrm{Re}\{k\}\mathrm{Im}\{k\} = \mathrm{Re}\{k\}\mathrm{Im}\{k\}$. Since the source medium (air) is lossless, $\mathrm{Im}\{k\} = 0$, and the hyperbola becomes $\mathrm{Re}\{k\}\mathrm{Im}\{k\} = 0$. The first branch cut is $\mathrm{Im}\{k_z\} = \mathrm{Im}\left\{\sqrt{k^2 - k^2}\right\} = 0$, which starts at the branch point, goes to the origin along the real axis and then goes to $-i\,1$ along the positive imaginary axis. The second branch cut is $\mathrm{Re}\{k_z\} = \mathrm{Re}\left\{\sqrt{k^2 - k^2}\right\} = 0$, which starts from the branch point and goes to -1 along the positive real axis [10], [24]. If any path of integration crosses the branch cut $\mathrm{Im}\{k_z\} = 0$, the imaginary part of k_z (i.e. $\mathrm{Im}\{k_z\}$) changes its sign, while crossing the $\mathrm{Re}\{k_z\} = 0$ branch cut will change the sign of $\mathrm{Re}\{k_z\}$. This is significant as the change in the sign of $\mathrm{Re}\{k_z\}$ will result in a wave travelling in opposite direction, and if $\mathrm{Im}\{k_z\}$ changes from being positive to negative, the wave's amplitude will increase exponentially with z, violating radiation condition.

We now describe two numerical methods for computing field components.

A. Simpson's method

Having taken necessary steps to overcome the problems mentioned above, it is possible to implement Simpson's method to evaluate the integrals [8], [10], [20]. As shown in Fig. 2, we start our integration from the point $k = 0 - i\ _i$, where $_i$ is a small positive number. This small imaginary offset will make the path of integration go along the fourth quadrant. Since the poles and the branch points reside in the first quadrant, such detour will ensure that no such points are

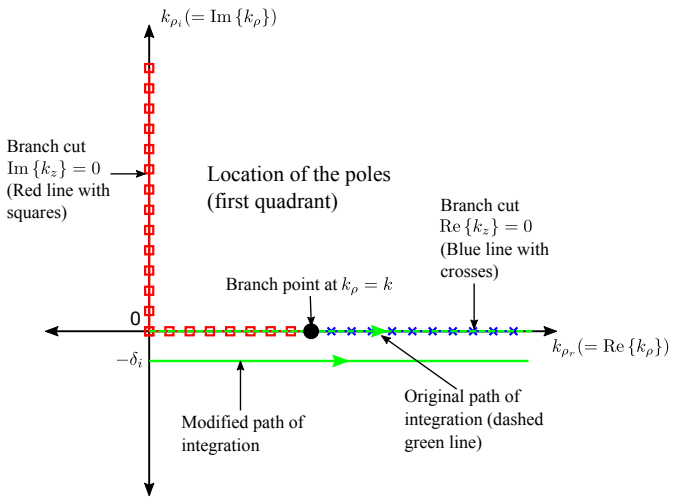

Fig. 2. Location of the poles and the branch point, and deformation of the path of integration

traversed. In our work, we choose $_i = \frac{0:01}{}$. It is well known [24] that the Bessel functions diverge for arguments with large negative imaginary part. The choice $_i = \frac{0:01}{}$ prevents this divergence by making $\mathrm{Im}fk \quad g$ a small constant, $0{:}01$.

The increment is chosen $k = k_r = \frac{0:05}{}$ with $k_i = 0$, thereby making the path of integration parallel to the k_r axis. With increasing , the oscillations of the Bessel and Hankel functions will be more rapid, and so in order to maintain accuracy of the computation of the integral, the sampling of the values of the integrand should be more dense. Our choice of such an inverse relation with will fit to the purpose as increasing will automatically make the sampling interval narrow.In this way the Simpson's rule is made robust to any frequency and nonzero receiver height, and the desired accuracy is a case of varying tolerance and increment.

The theoretical upper limit of the integral is 1. However, as $z \quad 0$, the exponential $e^{ik_z z}$ in (3) serve as a decaying factor when $jk\ j > k$ as $k_z = \sqrt{k^2 \quad k^2}$ becomes imaginary. So although the Bessel functions oscillate indefinitely, the integral will converge for sufficiently high values of the upper limit. A very important point to note is setting $z = 0$ will not allow this decay, so the integral will never converge. Hence this upper limit practically depends on k (which is proportional to the operating frequency) and z, the receiver height. At low frequency or high receiver height, the upper limit is small. We determine the upper limit by the method of convergence with a given tolerance of $10^{\ 6}$.

B. DFT method

The discrete Fourier transform (DFT) method of numerical evaluation is described by [8], [25], [26], [36]. This method exploits the fact that although the integrals of the Bessel functions are not closed-form integrable, integrals of the following type have closed-form solutions as mentioned in [37]

$$\int_0^{\ 1} e^{\ ax} J(bx)dx$$

Here $J(x)$ can be any of $J_0(x)$, $J_1(x)$ or $N_0(x)$, and a is in general a complex number. The solutions are:

$$\int_0^{\ 1} e^{\ ax} J\ (bx)dx = \frac{b}{p\overline{a^2+b^2}\quad a}; \quad = 0;1 \tag{9a}$$

$$\int_0^{\ 1} e^{\ ax} N_0(bx)dx = \frac{2}{p\overline{a^2+b^2}} \ln\frac{a+p\overline{a^2+b^2}}{b} \tag{9b}$$

We first use (5) to replace the derivatives of the Hankel functions in the integrals of (3) with ordinary Hankel functions. The integrals will have any of the following three representations:

$$\begin{aligned} T^E_{H_0} &= \int_{\ 1}^{\ 1} E(k\ ) H_0^{(1)}(k\quad) dk \\ &= 2i \int_0^{\ 1} E(k\ ) N_0(k\quad) dk \end{aligned} \tag{10a}$$

$$\begin{aligned} T^O_{H_0} &= \int_{\ 1}^{\ 1} O(k\ ) H_0^{(1)}(k\quad) dk \\ &= 2 \int_0^{\ 1} O(k\ ) J_0(k\quad) dk \end{aligned} \tag{10b}$$

$$\begin{aligned} T^E_{H_1} &= \int_{\ 1}^{\ 1} E(k\ ) H_1^{(1)}(k\quad) dk \\ &= 2 \int_0^{\ 1} E(k\ ) J_1(k\quad) dk \end{aligned} \tag{10c}$$

Here $E(k\ )$ and $O(k\ )$ signify even and odd functions of k. Equation (9a) is applicable for (10b) and (10c), while (9b) is applicable for (10a). In general, the representation is

$$\begin{aligned} T_H &= \int_{\ 1}^{\ 1} h(k\ ) H^{(1)}(k\quad) dk \\ &= 2 \int_0^{\ 1} h_1(k\ ) J(k\quad) dk \end{aligned} \tag{11}$$

Comparing (9) with (10) and (11), we have $x = k$, $b = \ $. Since there is an inclusion of $e^{\ ak}$ in the integrals of (9), we change (11) the following way:

$$T = 2 \int_0^{\ 1} e^{ak}\ h_1(k\ ) e^{\ ak}\ J(k\ ) dk \tag{12}$$

Let $a = a_r + ia_i$. The choice of a_r is arbitrary as long as $a_r > 0$, and we set $a_r = \frac{z}{2}$, where z is the receiver height [8], [25]. We also set $a_i = \ 2\ f$, which allows us to use the DFT transformation from k domain to f domain. From (12) we obtain

$$T = 2 \int_0^{\ 1} e^{(a_r+ia_i)k}\ h_1(k\ ) e^{\ (a_r+ia_i)k}\ J(k\ ) dk \tag{13}$$

Setting $g(k\ ) = 2e^{a_r k}\ h_1(k\ )$, we have

$$\begin{aligned} T &= \int_{\ 1}^{\ 1} g(k\ ) e^{ia_i k}\ e^{\ (a_r+ia_i)k}\ J(k\ ) dk \\ &= \int_0^{\ 1} g(k\ )\ e^{\ a_r k}\ J(k\ ) dk \end{aligned} \tag{14}$$

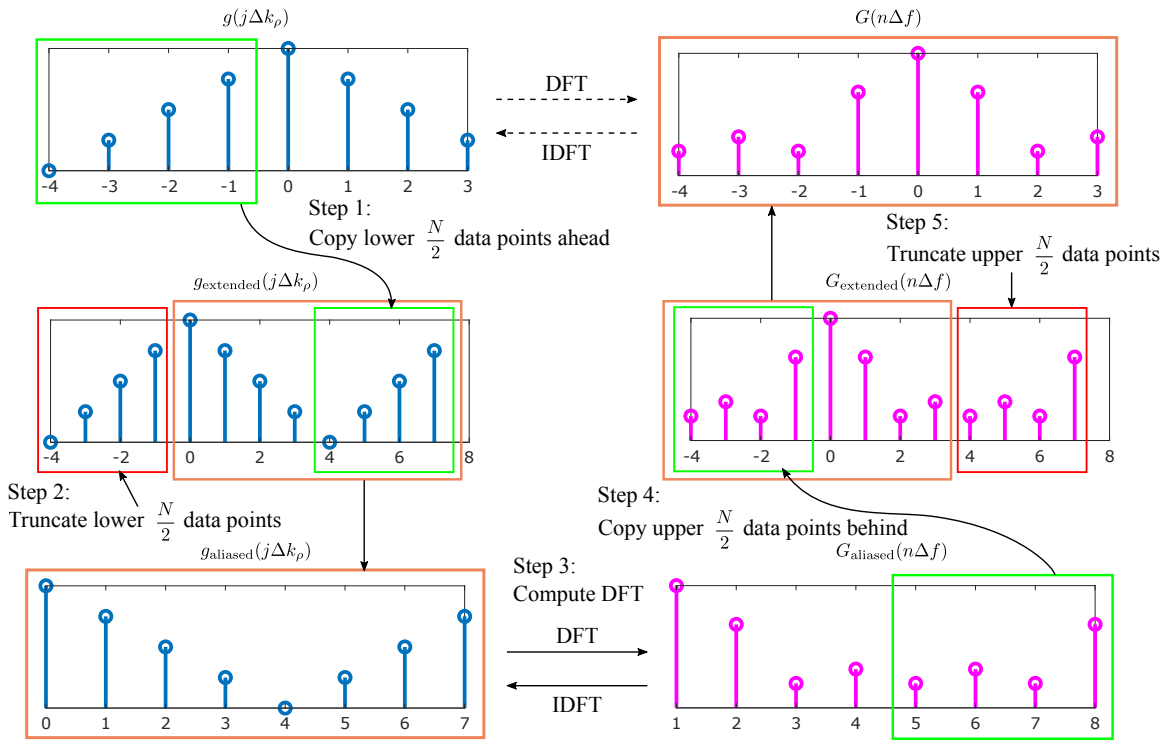

Fig. 3. Demonstration of obtaining proper $G(n\ \ f)$ from $g(j\ \ k\ )$ using 8-point DFT

Let $G(f)$ be the Fourier transform of $g(k\ )$, i.e.

$$G(f) = \int_{-1}^{1} g(k\ )e^{\ i2\ \ fk}\ dk \tag{15}$$

The N-point sampled versions of $g(k\ )$ and $G(f)$ are $g(j\ \ k\ )$ and $G(n\ \ f)$, respectively, where $k\ = \frac{0:1}{\ } =$ the sampling interval for k and $f = \frac{1}{N\ \ k}$. We can represent them as a DFT pair with the following expression

$$\begin{aligned} g(j\ \ k\ ) &= \frac{1}{N}\sum_{n=\ \frac{N}{2}}^{\frac{N}{2}X1} G(n\ \ f)e^{i\frac{2\ jn}{N}} \\ &= \frac{1}{N}\sum_{n=\ \frac{N}{2}}^{\frac{N}{2}X1} G(n\ \ f)e^{i2\ jn\ \ f\ \ k} \\ &\quad \frac{1}{N}\sum_{n=\ \frac{N}{2}}^{\frac{N}{2}X1} G(n\ \ f)e^{ia_ik} \end{aligned} \tag{16}$$

where $j;n\ 2\ \mathbb{Z}$, $\frac{N}{2}\ \ j;n\ \ \frac{N}{2}\ \ 1, k\ \ \ j\ \ k$ and $a_i\ \ 2\ n\ \ f$. However, in order for (16) to hold, we must ensure that the function $g(j\ \ k\ )$ sufficiently approaches zero outside the summation interval (i.e. $g(j\ \ k\ )\ \ 0$ for $j > \frac{N}{2}\ \ 1$). Otherwise the DFT will work upon a truncated version of $g(j\ \ k\ )$, which is undesirable. In our experiment, we choose $N = 2^{14}$. Although this high value will slightly increase the computation time, it will guarantee that the function $g(j\ \ k\ )$ is close to 0 outside the considered interval. Now substituting (16) in (14) yields

$$\begin{aligned} T &= \frac{1}{N}\int_0^{\ 1} \left\{ \sum_{n=\ \frac{N}{2}}^{\frac{N}{2}X1} G(n\ \ f)e^{ia_ik} \right\} e^{\ a_rk}\ \mathrm{J}(k\ )\,dk \\ &= \frac{1}{N}\sum_{n=\ \frac{N}{2}}^{\frac{N}{2}X1} G(n\ \ f) \int_0^{\ 1} e^{\ (a_r\ \ ia_i)k}\ \mathrm{J}(k\ )\,dk \\ &= \frac{1}{N}\sum_{n=\ \frac{N}{2}}^{\frac{N}{2}X1} G(n\ \ f) \int_0^{\ 1} e^{\ a\ k}\ \mathrm{J}(k\ )\,dk \end{aligned} \tag{17}$$

The term inside the curly braces of (17) can be closed-form transformed based on the nature of J in (10) following the transformation rules mentioned in (9).

There is one important point to note for evaluating $G(n\ \ f)$. Although for our computation we need N data-points of $g(k\ )$ ranging from $\frac{N\ \ k}{2}$ to $\frac{N}{2}\ \ 1\ \ k$, most DFT routines will interpret the N values as if in the range of 0 to $(N\ \ 1)\ \ k$. This will result in an aliased version of $G(n\ \ f)$ [36]. Fig. 3 shows a way to solve this problem. We first consider $g(j\ \ k\ )$ to be periodic after N samples, and then alias $g(j\ \ k\ )$ from $\frac{N}{2}\ \ k$ to $(N\ \ 1)\ \ k$, which correspond to $g(j\ \ k\ )$ from $\frac{N\ \ k}{2}$ to $\ \ k$. This new function $g_{\text{aliased}}(j\ \ k\ )$ is passed into the DFT routine, and we find $G_{\text{aliased}}(n\ \ f)$. We take a similar procedure with $G_{\text{aliased}}(n\ \ f)$, copy the upper $\frac{N}{2}$ samples backwards, and obtain $G(n\ \ f)$.

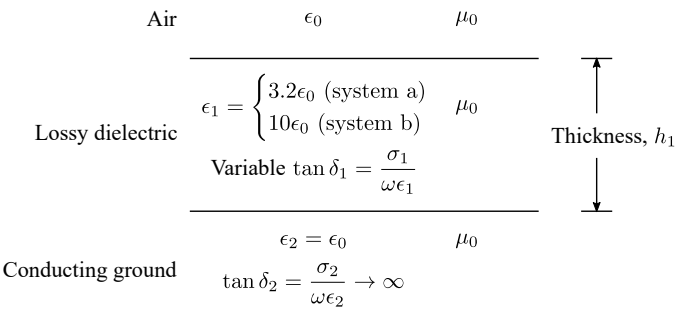

Fig. 4. Geometric configuration of systems a and b

IV. Simulation Results and Discussions

In this section, we present computational results and also investigate the feasibility of dielectric characterization in order to determine the dielectric constants, loss values and the thickness. The section is divided into three subsections. In subsection A, we present the variations of the field components with all the characterization variables and external factors such as the frequency and receiver distance. In subsection B, the physical interpretation of the proposed near-field interferometry is provided and the limitations are described. In subsection C, we perform analytical measurements on a sea ice model [35] and discuss the feasibility of estimating sea ice thickness from the near-field response.

For the analytical computation, we consider three layered systems terminated by a very high conductive infinite half space and choose two different geophysical possibilities. In the first system, the subsurface is assumed to have a dielectric constant of 3.2, similar to the glacier structure in [2], and the second system has a dielectric constant of 10, similar to the lossy ground values presented in [13]. For ease of discussion, we refer the glacier system as "system a" and the lossy ground system as "system b". The arrangement is schematically shown in Fig. 4. The source is placed on the upper dielectric surface ($d_0 = 0$), the receiver is placed at a height 2 m above the surface. For each system, we choose three values of the loss tangent $\tan\ _1$ of the dielectric as 5, 50 and 500, each defined at 1 MHz, to demonstrate the feasibility and limitations to characterize thickness and dielectric properties using the near-field interferometry.
We have computed the fields using both Simpson's and DFT methods and the results are identical. However, the Simpson's rule has the complexity $O(n_1)$, n_1 is the number of data points in the quadrature rule for convergence, whereas the DFT rule (if FFT is used) has the complexity $O(n_2 \log_2(n_2))$, n_2 being the number of FFT points. In the near fields, and for the given operating configurations, the Simpson's rule is found to converge faster than the DFT routine, and therefore computationally more efficient.

A. Investigation of field variations with different parameters

1) **Variation with internal parameters:**
We investigate the variation of H_z with the above mentioned loss tangent values for both system a and b.

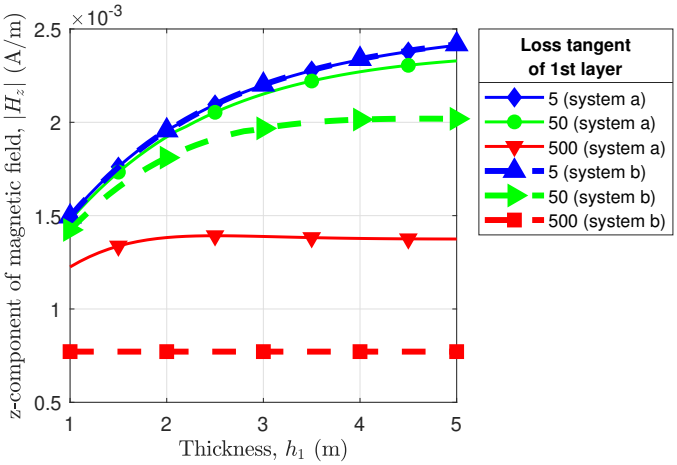

Fig. 5. Variation of $|H_z|$ with the subsurface thickness h_1, for systems a and b with different values of loss tangent ($\tan\ _1$) at 1 MHz. Receiver location is at $= 5m$, along broadside

The results are presented in Fig. 5 for different thickness of the dielectric medium. The following trends can be identified:

The fields produce a monotonic change with variable subsurface thicknesses and after certain limits, becomes invariant to them. These limiting values, after which the fields becomes thickness invariant is directly related with the loss tangent of the medium, and on the dielectric constant. For $\tan\ _1 = 5$, we see a monotonic rise in the field components and the fields are capable of capturing thickness changes above $5m$. For an increased loss tangent of 50, system a is still capable of showing field variations of similar range, but system b appears to become thickness invariant for values above $3m$. For a very high loss tangent value of 500, we find that system a is only varying with thickness up to $2m$ while system b shows a flat line, indicating the field measurements do not show any information on the medium thickness.
Comparing system a (the solid lines) with system b (the dashed lines), we can identify how the near field measurement is able to distinguish the two dielectrics. The variation of fields with various systems, also appear directly related to the loss tangent values. For $\tan\ _1 = 5$ we see that the field variations appear to be invariant with the two systems, despite being able to respond to large thicknesses. For $\tan\ _1 = 50$ we find a very significant variation of field components with changing dielectric properties, as well as appreciable changes with medium thickness. Finally, for $\tan\ _1 = 500$, the fields appear to show maximum variation between the two systems, despite being almost invariant to thickness. Each of the two systems shows different monotonic field variation with change of medium loss tangent, and hence the near field values are sensitive to the medium loss as well.

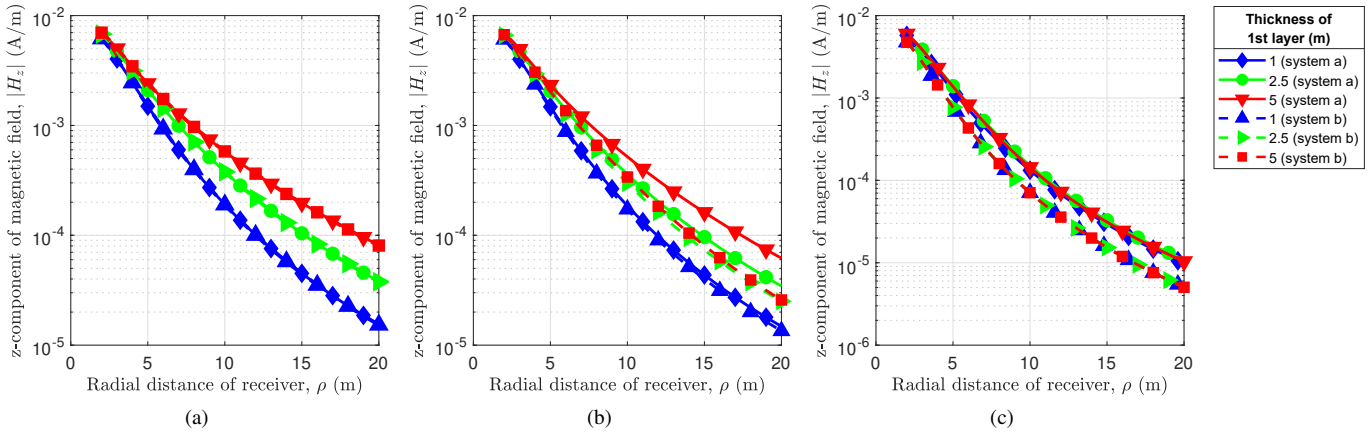

Fig. 6. Variation of $|H_z|$ with radial distance of receiver, , along the broadside direction of the source antenna for systems a and b with different values of thickness, h_1. The values of tan $_1$ are (a) 5, (b) 50 and (c) 500 respectively

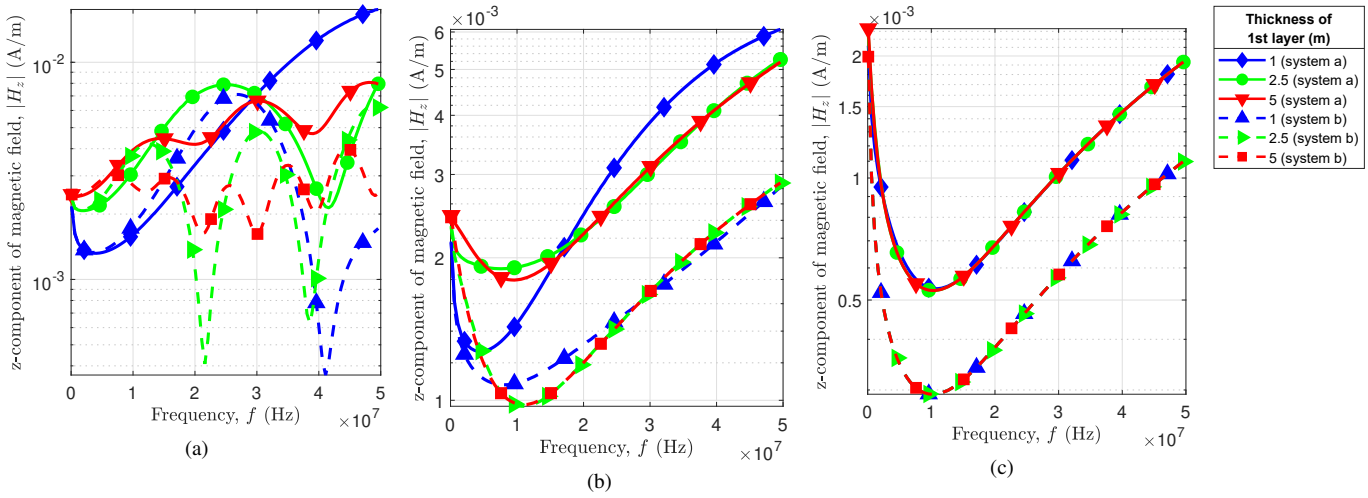

Fig. 7. Variation of $|H_z|$ with frequency of the source antenna for systems a and b with different values of subsurface thickness, h_1.The values of tan $_1$ are (a) 5, (b) 50 and (c) 500 respectively. Receiver is at = 5m, along broadside of source antenna.

From these observations it is clear that the near field measurements can distinguish both the medium dielectric properties and thickness, and the resolution is directly related with the loss tangent values of the medium. Too high or too low values of the loss tangent result in two limiting cases, which will be discussed in subsection B.

For now, we emphasize upon the observable variations and seek to capture them by sweeping the receiver location and the operating frequency.

2) **Variation with the external parameters:**

Now, we observe the field variations by varying the receiver distance from the source. Since H_z maximizes at the broadside direction, our receiver location is swept along that direction. The results are presented in Fig. 6. When tan $_1$ = 5 (Fig. 6a), we observe good field variations with varying thickness, but the coalescence of the solid lines with the dashed lines indicate very little variation with dielectric properties. For tan $_1$ = 50 (Fig. 6b), the field variation due to dielectric properties and thickness is much more prominent. However, for system b we see that the field values coalesce for thickness above 2:5m. For tan $_1$ = 500 (Fig. 6c), the difference between systems a and b is distinguishable, but the radial sweeps (among the same system) for different thicknesses coalesce and it implies that there is no available information on medium thickness. These observations completely agree with those presented in Fig. 5 and confirm that the internal variations of dielectric properties can be captured by external measurements.

We now investigate the variation of H_z by varying frequencies in the range 1-50 MHz for different thicknesses and loss tangents of systems a and b. Although this is a multi-frequency measurement, we can still expect that the general trends observed above will be maintained. For computation, we chose an arbitrary receiver location of 5m, along broadside.

First, We determine an equivalent conductivity of the system using the relation:

$$_1 = \tan\ _1 \, ! \ _{1;r\ 0}$$

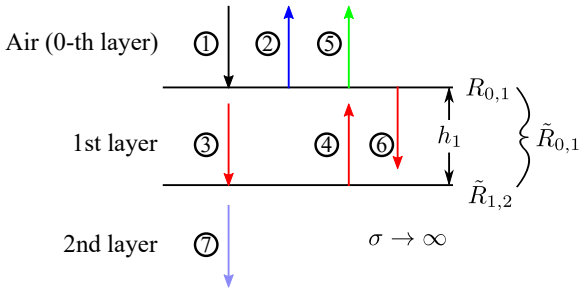

Fig. 8. Schematic representation of the operating principle in the low frequency near field region

and assume this conductivity value is a constant under our low frequency range. The results of the frequency sweep is presented in Fig. 7.

For $\tan_1 = 5$ (Fig. 7a), we can see that the fields vary very significantly with changing thickness, and they appear to be very different for the systems a and b. The values and patterns appear to be distinct for each medium's dielectric properties. For an elevated loss tangent of 50 (Fig. 7b), the ripple tends to smooth out and the responses appear to be more monotonic for both systems. The fields still appear to be quite distinctive with the medium dielectric properties, but the variations become invariant after a certain thickness. This thickness value does not vary much with frequency. Again, system b appears to become invariant to thickness much quicker, compared to system a. For $\tan_1 = 500$ (Fig. 7c), the fields appear to be completely invariant of thickness, but showing changes for different dielectric properties. These measurements keep integrity with the observations in Fig. 6c that at high loss values the field measurement cannot characterize thickness, but changes with dielectric system; however Fig. 7a suggests that multi-frequency measurements may provide more information on the medium dielectric behaviours at low loss tangent values, which appeared absent in Fig. 6a.

Having discussed the possibility of near field interferometry to characterize dielectrics, we present the reasons behind the possibility at the first place, together with a clear interpretation of the two limiting cases in the next subsection.

B. A physical interpretation of the near field approach: the limits on the characterization problem

In this section we present a physical and mathematical interpretation behind the limits of the loss tangent, which is the primary governor of the near field interferometry. Let's consider the ray schematics of a single decomposed planewave component of any arbitrary k_z as shown in Fig. 8, which can be generalized to all the k_z present in the total response.

A fraction of the incident wave ① is reflected back from the top surface as ②, conveying information on subsurface dielectric. The remaining wave ③ propagates inside the dielectric and reflects from the bottom surface as ④, conveying information on the medium thickness and loss tangent. ⑦ propagates through the infinite halfspace, and the remaining wave ⑥ undergoes multiple reflections inside the dielectric. The wave propagating to the receiver is ⑤. Both systems a and b are terminated by highly conducting media, and therefore if we consider regular, non evanescent waves ($jk\,j \quad k$), then there is always almost full reflection from the lower surface. The unwanted evanescent wave contributions ($jk\,j > k$) can be easily suppressed by choosing a large enough receiver height from the top surface [10]. Now, depending on the lossy nature of the subsurface, we discuss the following limiting cases:

Case 1: If the subsurface loss tangent is too low, then the reflection from the top surface ② is usually very low compared to bottom reflected wave ④. When ④ is incident on the top interface from below, there will always be less reflection and high transmission, and hence ⑤ will have a much higher value compared to ② and suppress it. As a result, the total reflection coefficient will appear to be invariant of the subsurface dielectric properties. In this limit, the variation with thickness is observable as ⑤ contains the thickness information in its phase due to the path covered by ③ and ④ inside the subsurface. Therefore, this is the limit where characterizing the thickness is possible, but not the dielectric properties.

Case 2: If the subsurface loss tangent and the thickness are high enough, then we observe a completely different phenomenon. The high loss tangent of the subsurface will make it a good reflector, which results in a high magnitude of ② and a low magnitude of ③. If the thickness is a little large, ③ will diminish very quickly as it propagates and reflects inside. Then ④ and ⑤ will be very negligible, while ② alone will dominate and mostly determine the total reflection coefficient. In this limit, the bottom infinite ground will be "masked", there will be no available information on the thickness, and the three layered structure will resemble a two layered halfspace. As the reflection is entirely dominated by the top surface, it will vary with the dielectric properties of the subsurface. Hence, the dielectric properties can be determined but the thickness measurement cannot be performed.

Mathematically these two limiting cases can be explained as follows. For a three layered system, the reflection coefficient (for both TM or TE) can be viewed as

$$\tilde{R}_{0;1} = \frac{R_{0;1} + \tilde{R}_{1;2} e^{\ 2ik_{z;1}h_1}}{1 + R_{0;1}\tilde{R}_{1;2} e^{\ 2ik_{z;1}h_1}}: \tag{18}$$

For case 1, $jR_{0;1}j << \tilde{R}_{1;2} \quad 1$. So we can ignore the terms associated with $jR_{0;1}j$ from both the numerator and denominator of (18), and the the total refection coefficient can be obtained as $\tilde{R}_{0;1} \quad \tilde{R}_{1;2} e^{\ 2ik_{z;1}h_1}$. Since there is no term involving $R_{0;1}$, the near field cannot characterize the dielectric properties in this limiting condition.

For case 2, the loss and/or the thickness are large enough and $jR_{0;1}j$ cannot be neglected. To the contrary, the medium losses make $2ik_{z;1}$ acquire a large real value, which is scaled by the medium thickness h_1. Hence we can consider the exponential terms in (18) to be very small. Suppressing the exponential terms yields $\tilde{R}_{0;1} \quad R_{0;1}$. Since there is no term containing h_1, the reflection coefficients and fields become invariant to

thickness in this limiting condition.

Within these two limits, there exist an optimum range of loss tangents, for which the reflection coefficient and the fields respond to all three characterization variables and none of the terms in (18) can be ignored. It is the range where the field measurements can characterize all three unknowns, as observed in Figs 5 and 6b. This optimum range of loss tangent is also dependent on the thickness of the substance we are interested at. For large thickness, even a low loss tangent can cause sufficient loss during propagation, while for small thickness, the waves will not attenuate completely for large loss tangents. Finally, we note that the highly conductive bottom ground is responsible for the case 1 limits. If the system was terminated by an ordinary dielectric instead, then this limit would have been absent and dielectric characterization would have been possible even for low loss tangent values. However, a good fraction of waves would penetrate within the infinite ground (higher magnitude of ⑦) resulting in lesser magnitudes of ④ and ⑤ which convey information on the medium thickness. Therefore, the resolution of the field variations with changing thickness would have been significantly lower.

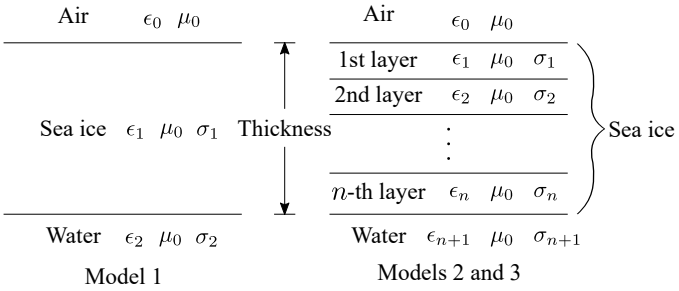

Fig. 9. Sea ice models presented in [35]

C. Investigation on a sea ice model

As a possible method for medium characterization, we perform similar computations on a multilayered sea ice using the three models in [35]. The schematic diagrams of the models is shown in Fig. 9. Model 1 considers the air-sea ice-sea water system as a simple three layered system. Sea ice can be considered as a more lossy dielectric substance compared to the glacier ("system a") because of its inherent salinity, while sea water can be viewed as a highly conducting infinite halfspace, similar to the conducting grounds in [2]. For model 1, the loss tangent at 1 MHz is approximately 55, which is in the optimum range in order to determine the sea ice properties and thickness using near field interferometry. Models 2 and 3 consider sea ice to be a more complex graded structure, although the dielectric and loss variations are not highly different among them.

First, we investigate the variations of H_z with thickness, for each of the models. The results are presented in Fig. 10. All three models show a monotonic increase of H_z with thickness, while the profiles also appear different for each of the models.

Next we perform a radial sweep similar to Fig. 6 to capture the changes with variable thickness of the sea ice models. We choose the Model 1 to investigate the possibility, and the field

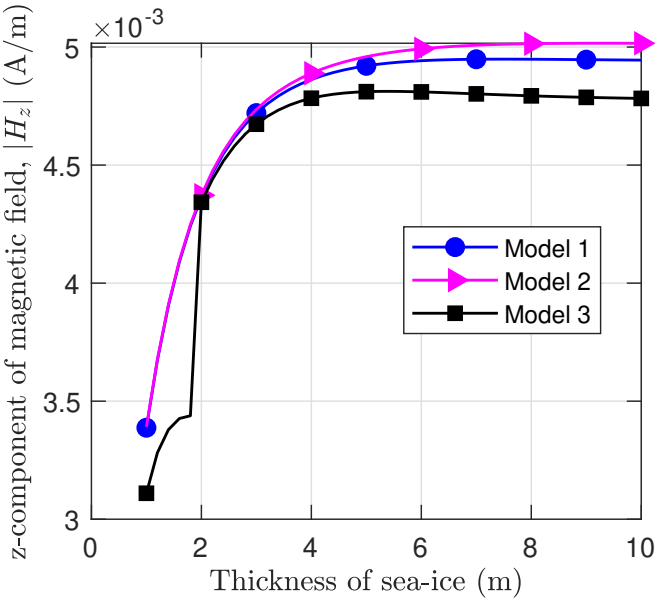

Fig. 10. Variation of H_z with thickness of sea ice. The variations for the three models in [35] are shown.

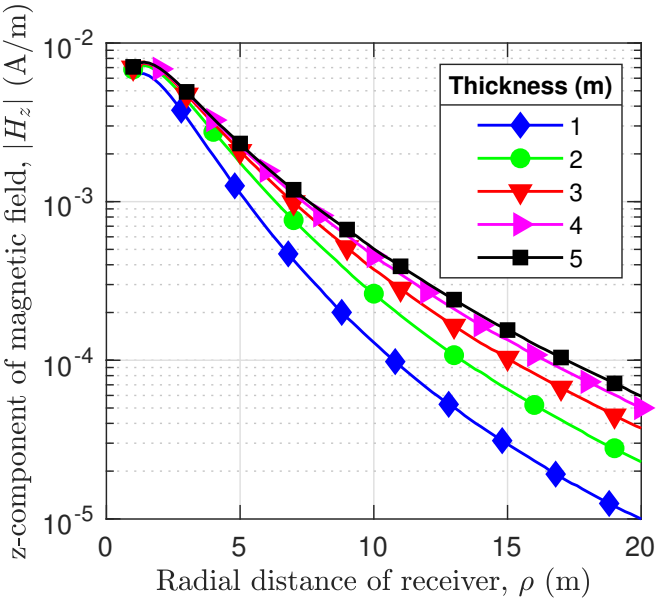

Fig. 11. Variation of H_z with radial distance ( ) of receiver for different thicknesses of sea ice. Model 1 of [35] is used.

values are presented in Fig. 11. The graphs for the different thicknesses are sufficiently distinguishable, for thickness up to 5 meters. The practical sea ice bulk has a thickness in similar ranges, therefore the near field interferometry can be a promising method to determine the sea ice thickness.

V. Conclusion

In this paper, we have investigated the feasibility of the near field interferometry to determine the dielectric properties and thickness of any possible geophysical substance. The analytical results show that it is possible to determine the thickness of the substance when the loss is very low, and the

dielectric properties only when the loss is very high. Between these two limits of loss, there exists an optimum range where it is possible to determine all three characterization unknowns. A physical and mathematical explanation is presented on the principle which is governing the field variations and the limits. A possible investigation was also done to measure thickness of a given sea ice model, whose dielectric properties change with each model type. The fields showed monotonic changes for each type and varying thickness, which has been extracted by an external radial sweep. These analytical results suggest the near field interferometry has the potential to be a very useful tool to characterize sea ice. Our future plans include the physical realization of the proposed method, which can go a long way towards mapping sea ice in the polar regions. A successful realization can have several useful applications in areas such as maritime navigation and climatology.

ACKNOWLEDGEMENT

This work has been supported by the Office of Naval Research Global, London, UK [grant N62909-19-1-2013] as part of the NICOP project "Non-invasive measurement of sea ice thickness using low frequency EM waves".

REFERENCES

[1] A. P. Annan, "Radio Interferometry Depth Sounding: Part I-Theoretical Discussion," *Geophysics*, vol. 38, no. 3, pp. 557–580, Jun. 1973.

[2] J. R. Rossiter, G. A. LaTorraca, A. P. Annan, D. W. Strangway, and G. Simmons, "Radio Interferometry Depth Sounding: Part II - Experimental Results," *Geophysics*, vol. 38, no. 3, pp. 581–599, Jun. 1973.

[3] A. P. Annan, W. M. Waller, D. W. Strangway, J. Rossiter, J. D. Redman, and R. Watts, "The electromagnetic response of a low-loss, 2-layer, dielectric earth for horizontal electric dipole excitation," *Geophysics*, vol. 40, no. 2, pp. 285–298, Apr. 1975.

[4] W. C. Chew and J. A. Kong, "Electromagnetic field of a dipole on a two-layer Earth," *Geophysics*, vol. 46, no. 3, pp. 309–315, Mar. 1981.

[5] L. Tsang, J. A. Kong, and G. Simmons, "Interference patterns of a horizontal electric dipole over layered dielectric media," *Journal of Geophysical Research (1896-1977)*, vol. 78, no. 17, pp. 3287–3300, Jun. 1973.

[6] DaHan Liao and K. Sarabandi, "Near-earth wave propagation characteristics of electric dipole in presence of vegetation or snow layer," *IEEE Transactions on Antennas and Propagation*, vol. 53, no. 11, pp. 3747–3756, Nov 2005.

[7] W. C. Chew and J. A. Kong, "Asymptotic approximation of waves due to a dipole on a two-layer medium," *Radio Science*, vol. 17, no. 3, pp. 509–513, May 1982.

[8] L. Tsang, R. Brown, J. A. Kong, and G. Simmons, "Numerical evaluation of electromagnetic fields due to dipole antennas in the presence of stratified media," *Journal of Geophysical Research (1896-1977)*, vol. 79, no. 14, pp. 2077–2080, May 1974.

[9] "Chapter vi - problems of radio," in *Partial Differential Equations in Physics*, ser. Pure and Applied Mathematics, A. Sommerfeld, Ed. Elsevier, 1949, vol. 1, pp. 236 – 296.

[10] W. C. Chew, *Waves and Fields in Inhomogeneous Media*. New York, NY: IEEE Press, 1995, ch. 1, 2.

[11] Sommerfeld identity.

[12] "Applied mathematics and mechanics: An international series of monographs," in *Waves in Layered Media*, ser. Applied Mathematics and Mechanics, L. Brekhovskikh, Ed. Elsevier, 1980, vol. 16.

[13] J. R. Wait, *Electromagnetic Waves in Stratified Media*, 2nd ed. Oxford: Pergamon Press, 1970, ch. 1,2.

[14] J. A. Kong, *Electromagnetic Wave Theory*. New York, NY: John Wiley & Sons, 1986.

[15] ——, "Electromagnetic fields due to dipole antennas over stratified anisotropic media," *GEOPHYSICS*, vol. 37, no. 6, pp. 985–996, 1972.

[16] C.-M. Tang, "Electromagnetic fields due to dipole antennas embedded in stratified anisotropic media," *IEEE Transactions on Antennas and Propagation*, vol. 27, no. 5, pp. 665–670, Sep. 1979.

[17] Y. S. Kwon and J. J. H. Wang, "Computation of hertzian dipole radiation in stratified uniaxial anisotropic media," *Radio Science*, vol. 21, no. 6, pp. 891–902, Nov. 1986.

[18] W. C. Chew, "A quick way to approximate a sommerfeld-weyl-type integral (antenna far-field radiation)," *IEEE Transactions on Antennas and Propagation*, vol. 36, no. 11, pp. 1654–1657, Nov 1988.

[19] J. Wait, "Asymptotic theory for dipole radiation in the presence of a lossy slab lying on a conducting half-space," *IEEE Transactions on Antennas and Propagation*, vol. 15, no. 5, pp. 645–648, Sep. 1967.

[20] J. Kong, L. Tsang, and G. Simmons, "Geophysical subsurface probing with radio-frequency interferometry," *IEEE Transactions on Antennas and Propagation*, vol. 22, no. 4, pp. 616–620, July 1974.

[21] N. Bleistein and R. Handelsman, *Asymptotic Expansions of Integrals*, ser. Dover Books on Mathematics Series. Dover Publications, 1986.

[22] N. Bleistein, "Uniform asymptotic expansions of integrals with stationary point near algebraic singularity," *Communications on Pure and Applied Mathematics*, vol. 19, no. 4, pp. 353–370, Nov. 1966.

[23] ——, "Uniform asymptotic expansions of integrals with many nearby stationary points and algebraic singularities," *Journal of Mathematics and Mechanics*, vol. 17, no. 6, pp. 533–559, 1967.

[24] A. I and M. Venkatapathi, "Analysis of numerical solutions to sommerfeld integral relation of the half-space radiator problem," *Applied Numerical Mathematics*, vol. 106, pp. 79 – 97, 2016.

[25] J. J. H. Wang, "General method for the computation of radiation in stratified media," *IEE Proceedings H - Microwaves, Antennas and Propagation*, vol. 132, no. 1, pp. 58–62, February 1985.

[26] J. Kong, Liang-Chi Shen, and L. Tsang, "Field of an antenna submerged in a dissipative dielectric medium," *IEEE Transactions on Antennas and Propagation*, vol. 25, no. 6, pp. 887–889, November 1977.

[27] L. N. G. Filon, "Iii.—on a quadrature formula for trigonometric integrals," *Proceedings of the Royal Society of Edinburgh*, vol. 49, p. 38–47, 1930.

[28] E. Tuck, "A simple "filon-trapezoidal" rule," *Mathematics of Computation*, vol. 21, no. 98, pp. 239–241, 1967.

[29] D. Bubenik, "A practical method for the numerical evaluation of sommerfeld integrals," *IEEE Transactions on Antennas and Propagation*, vol. 25, no. 6, pp. 904–906, November 1977.

[30] M. Siegel and R. W. P. King, "Electromagnetic fields in a dissipative half-space: A numerical approach," *Journal of Applied Physics*, vol. 41, no. 6, pp. 2415–2423, 1970.

[31] J. Hunziker, J. Thorbecke, and E. Slob, "The electromagnetic response in a layered vertical transverse isotropic medium: A new look at an old problem," *GEOPHYSICS*, vol. 80, no. 1, pp. F1–F18, 2015.

[32] J. Hunziker, E. Slob, Y. Fan, R. Snieder, and K. Wapenaar, "Electromagnetic interferometry in wavenumber and space domains in a layered earth," *GEOPHYSICS*, vol. 78, no. 3, pp. E137–E148, 2013.

[33] J. Hunziker, J. Thorbecke, and E. Slob, *Manual for the software EMmod*, emmod models the electromagnetic response of a layered VTI medium.

[34] Emmod.

[35] M. S. Islam, S. Shafi, and M. A. Haque, "Electromagnetic characterization of sea ice using low frequency electromagnetic waves," in *Proc. The 7th Advanced Electromagnetics Symposium (AES 2019)*, Lisbon, Portugal, Jul. 2019, pp. 290–294.

[36] J. Cooley, P. Lewis, and P. Welch, "Application of the fast fourier transform to computation of fourier integrals, fourier series, and convolution integrals," *IEEE Transactions on Audio and Electroacoustics*, vol. 15, no. 2, pp. 79–84, June 1967.

[37] I. S. Gradshteyn and I. M. Ryzhik, *Table of Integrals, Series, and Products*, fourth corrected and enlarged edition ed. San Diego, California: Academic Press, 1980, pp. 707–708, incorporating the fourth edition prepared by Yu. V. Geronimus and M. Yu. Tseytlin.

M. Shifatul Islam completed his B.Sc. in electrical and electronic engineering from Bangladesh University of Engineering and Technology in March, 2018.

He is currently working as a Research and Development Engineer in Anyeshan Limited, and also pursuing his M.Sc. in electrical and electronic engineering in Bangladesh University of Engineering and Technology. His interests and work area include theoretical and computational electromagnetism, electromagnetics in geophysical and biomedical applications, antennas and metamaterials.

Sadman Shafi received the B.Sc. degree in electrical and electronic engineering from Bangladesh University of Engineering and Technology, Dhaka, Bangladesh, in 2017. He is currently a Research and Development Engineer with Anyeshan Limited, Dhaka, Bangladesh. His research interests include computational electromagnetics, quantum information and communication.

Md. Imrul Hasan received the B.Sc. degree in 2016. He is currently pursuing his Ph.D. and working as a Research Assistant at WiCoRe Lab at the University of Texas at Dallas, USA. His research interests include non-invasive evaluation using electromagnetic and acoustic waves, development of robust direction finding (DF) algorithms, and 5G communication systems.

Mohammad Ariful Haque received the B.Sc., M.Sc., and Ph.D. degrees in electrical and electronic engineering all from the Bangladesh University of Engineering and Technology (BUET), Dhaka, Bangladesh, in 2003, 2005 and 2009, respectively.

In 2003, he joined BUET as a Lecturer in the Department of Electrical and Electronic Engineering. He is currently working as a Professor in the same department. He was a Postdoctoral Fellow with Concordia University, Montreal, QC, Canada, and received the ReSMiQ Post-Doctoral Fellowship Award in 2012. His research interest includes digital signal processing, deep learning and systems engineering.

Prof. Haque has published thirty five scientific articles in internationally recognized and refereed journals and conferences. He has supervised finalist teams of global competitions on signal, image and video processing organized by the IEEE Signal Processing Society at ICASSP and ICIP venues from 2014-2020, seven years in a row.